# Multi-grid tomographic inversion for breast ultrasound imaging

Cuiping Li[1], Alexander Stewart[3], Neb Duric[1,2]

[1]Delphinus Medical Technologies, 46701 Commerce Center Drive, Plymouth, MI 48170; Email: cli@delphinusmt.com
[2]Karmanos Cancer Institute, 4100 John R. Street, 4 HWCRC, Detroit, MI 48201
[3]IPA, 2930 bluff st # 332 Boulder, CO 80301

## ABSTRACT

A multi-grid tomographic inversion approach that uses variable grid sizes in both forward modeling and inverse process is proposed and tested on breast phantom data and breast ultrasound data. In iterative tomographic inversion, fine scale features are more sensitive to starting model than coarse scale features. The proposed multi-grid algorithm starts from coarse grids for both forward modeling and inverse process and gradually proceeds to fine grids, which can effectively suppress artifacts related to over iteration of fine scale features. Since the computational complexity of inverse problems increases with number of grid points in both forward model and inverse model, the proposed algorithm greatly reduces the computational cost in contrast to standard fixed-grid approaches. Both in vitro and in vivo results indicate that the proposed multi-grid methods result in significant improvement in the inverted sound speed and attenuation images compared to fixed-grid methods.

**Keywords**: Multi-grid tomography, breast ultrasound imaging.

## 1. INTRODUCTION

Recent studies have demonstrated the effectiveness of ultrasound tomography imaging in detecting breast cancer. However, the standard fixed-grid methods suffer from artifacts related to over-iterated fine scale features because fine scale features in breast images converge faster than coarse scale features. Another major barrier to the use of inverse problem techniques has been the computational cost of the standard fixed-grid methods. These computational challenges are only made more difficult by concurrent trends toward larger data sets and correspondingly higher resolution images.

Multi-grid tomography techniques have been widely investigated as a method not only to reduce the computational cost but the artifacts related to over iteration in the reconstructed images[1-25]. The techniques have ranged from simple coarse-to-fine approches[1,3,22-25], which initialize fine-scale iteration with coarse-scale solutions, to more sophisticated wavelet or multi-grid image model-based approaches, which have been applied to different aspects of image reconstruction and image analysis[2,4-21]. The multi-grid methods were originally developed for fast partial differential equation (PDE) solver[26-27] and later were applied to inverse problem[28-38].

The multi-grid methods can greatly reduce computational complexity including both memory requirements and temporal cost and achieve fast convergence because the non-uniform convergence rates for coarse scale features and fine scale features have been taken into consideration. Additionally, images reconstructed using the multi-grid methods are less prone to artifacts since coarse grid corrections remove low frequency error components more effectively than fine-scale corrections[25]. In this study, the breast ultrasound dataset acquired with a ring array is large and needs to be inverted in a short time window to satisfy clinical throughput. For fast computation, we explore the application of the multi-grid methods to simultaneously reconstructing both sound speed and attenuation distributions within the breast. To demonstrate the effectiveness of this methods, we have applied them to both in vitro and in vivo data acquired by the ring array.

In this paper, we discuss the multi-grid tomography techniques and explain how we apply them simultaneously to both breast sound speed and attenuation reconstructions. We demonstrate a few examples of inversion results and the comparisons to the corresponding fixed-grid tomograms.

Medical Imaging 2012: Ultrasonic Imaging, Tomography, and Therapy, edited by Johan G. Bosch, Marvin M. Doyley, Proc. of SPIE Vol. 8320, 83200R · © 2012 SPIE
CCC code: 1605-7422/12/$18 · doi: 10.1117/12.912854

## 2. METHODOLOGY

### 2.1 Data acquisition

Data was acquired using a clinical prototype located at Karmanos Cancer Institute (KCI) in Detroit, MI. The current prototype employs a ring array with 256 evenly distributed ultrasound sensors. Array elements sequentially emit fan beams of ultrasound signals towards the opposite side of the ring. The scattered (transmission) and backscattered (reflection) ultrasound signals are subsequently recorded by all 256 elements at a sampling rate of 8.33 MHz. The transmitted broadband ultrasound signal has a central frequency around 2 MHz. The ring array resides in a tank filled with water for proper coupling of the ultrasound signal (Fig. 1).

In this study, we acquired ultrasound data for one breast-mimicking phantom and over 300 patients with the ring array. These data are reconstructed using both the multi-grid methods and standard fixed-grid method. We will show some examples and compare images resulting from both methods.

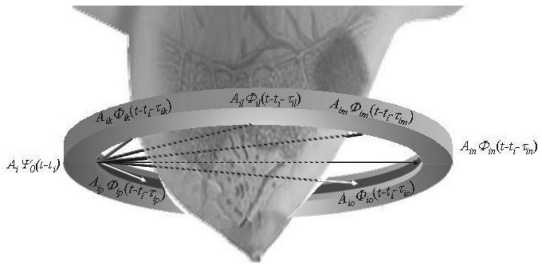

Figure 1. A schematic representation of the ring transducer.

### 2.2 Multi-grid tomography methods

Multi-grid tomographic inversion is based on the fact that fine scale features in breasts need fewer iterations to resolve and are more sensitive to starting model than coarse scale features. The tomographic inversion process starts from coarse forward model and inverse model grids, and gradually proceeds to fine model grids to solve the original finest-scale problem (Figure 2).

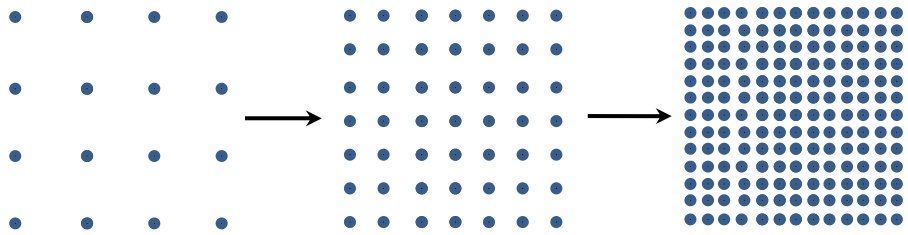

Figure 2. A schematic plot of the grid models showing the progress form coarse grid level to fine grid level.

*System equation*

The system equation that describes the transformation process in inverse problems is usually represented as equation (1).

$$Ax = b, \tag{1}$$

where $A$ is an $m$ x $n$ system matrix, which describe the system sensitivity, $x$ is an $n$ x 1 model parameter vector of the inverted pixel value (either sound speed or attenuation in our case), and $b$ is an $m$ x 1 vector of the measured data (either time-of-flight or integrated attenuation coefficient in the context of this paper).

In our study the size of the system in equation (1) is large, and $m$ and $n$ are in the order of tens of thousands. For a finer grid model equation (1) is usually ill-posed, with a nonempty null space, and more sensitive to the closeness of the starting model is to the true model. The Multi-grid tomography can tackle these problems in the following ways.

(i) The multi-grid methods start the tomographic process on a coarse grid model, which can greatly reduce the computational complexity of system equation (1);

(ii) System equation (1) discretized on coarse grid models will be better conditioned since there are more measurements than unknowns. Furthermore, inversion on a coarse grid model will provide a better starting model for later reconstruction on finer grids and reduce artifacts in the final images.

*Forward modeling*

Forward modeling of the multi-grid tomography generally follows that of the standard fixed-grid tomography methods[39]. The major feature that differentiates the multi-grid tomography from the fixed-grid tomography is that former starts the calculation of matrix $A$ (ray tracing) on a very coarse grid model and gradually updates the grid model to a finer and finer scale until the required grid level is reached, while the latter computes matrix $A$ using a fixed-grid model all through its iterations[39].

*Inverse problem*

Theories behind the inverse process are the same for both the fixed-grid tomography and the multi-grid tomography[39]. Both of them solve equation (1) for model parameters $x$ using measurement data $b$. The differences reside at the implementation level as described here. Unlike the fixed-grid tomography whose iterative reconstructions are based on a fixed grid model, the multi-grid tomography methods start from a coarse inverse grid model and update the model to a finer grid model after reaching the convergence on the coarse grid and restart the iterative inverse process. This process is repeated until the required grid size has been reached.

## 2.3 Simultaneous reconstruction of sound speed and attenuation using the multi-grid tomography

In our study, we simultaneously invert sound speed and attenuation images using the multi-grid methods as we explain below.

*Multi-grid sound speed inversion*

We reconstruct the sound speed images on three different grid levels, from coarse to finer, then to the required finest level. At each grid level, we iteratively solve the inverse problem by tracing the ray paths[39] on the corresponding grid level followed by solving the inverse problem using non-linear conjugate gradient (NLCG) method with restarting strategy[40]. The following are the details on how we reconstruct sound speed using the multi-grid methods.

(1) Starting from the coarse grid level, we iteratively solve the inverse problem on the current grid model until convergence is reached.

(2) We interpolate the sound speed image obtained from the final iteration at the current grid level onto the next grid level.

(3) Taking the interpolated sound speed image in (2) as the starting model, we iteratively solve the inverse problem at the next finer grid level until convergence is reached.

(4) Repeat (2) and (3) until the required grid level is reached.

*Simultaneous multi-grid attenuation inversion*

Attenuation images are inverted at the same time when we reconstruct the sound speed images. Unlike the non-linear sound speed reconstruction, inverting attenuation is a linear problem. Therefore, we solve it using LSQR method[41] instead of NLCG method[40]. The procedures to solve the multi-grid attenuation problem are described as follows.

(1) Starting from the very first coarse grid level, we reconstruct the attenuation using the final sound speed image at the same grid level.

(2) We interpolate the attenuation image reconstructed at the current grid level onto the next grid level.

(3) Taking the interpolated attenuation image in (2) as the starting model, we update the integrated attenuation coefficients when we trace the ray paths, and we reconstruct the attenuation using the final sound speed image at the current grid level.

(4) Repeat (2) - (4) until the required grid level is reached.

Figure 3 presents one example of sound speed reconstructions showing the progression of the multi-grid methods from coarse grid to fine grid.

(a)

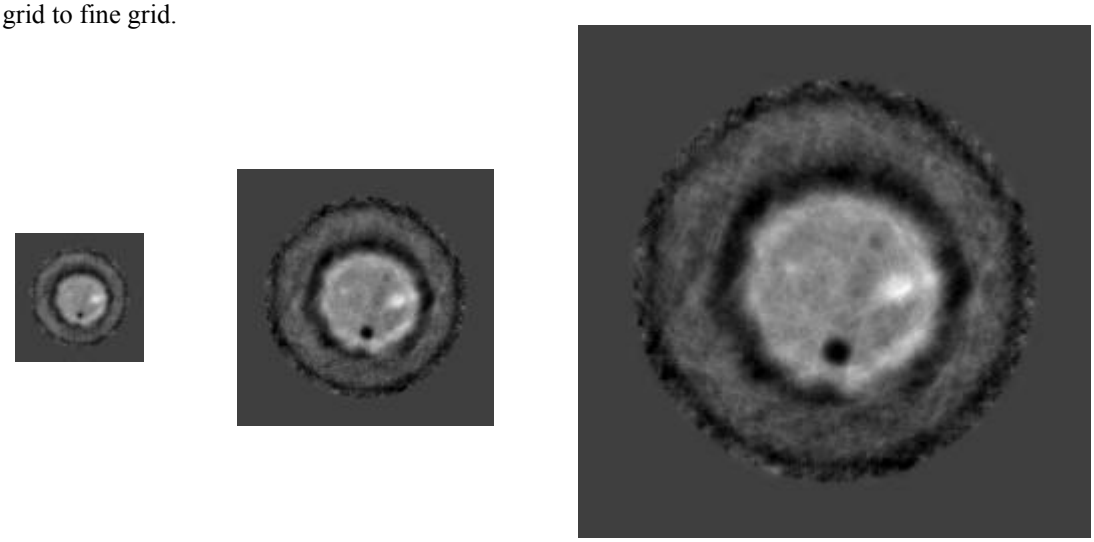

Figure 3. One example showing the progression of multi-grid methods from coarse grid to fine grid.

## 3. RESULTS

We apply the multi-grid tomography methods to both breast phantom data and patient breast data acquired with the ring array. We compare the obtained sound speed and attenuation images with those from the standard fixed-grid tomography. The results are present as follows.

### 3.1 Phantom study

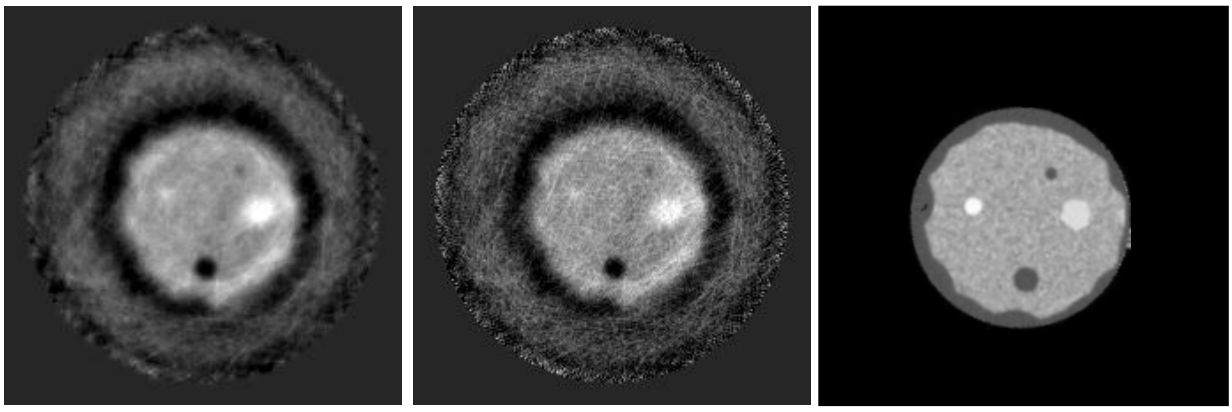


(a) Sound speed reconstruction with the multi-grid tomography

(b) Sound speed reconstruction with the fixed-grid tomography

(c) X-ray CT scan

Figure 4. (a) Sound speed reconstruction with the multi-grid tomography for the breast phantom. (b) Sound speed reconstruction with the fixed-grid tomography for the same cross section as in (a). (c) X-ray CT scan.

An initial phantom study was conducted to evaluate the performance of the multi-grid tomography methods. The breast phantom was built by Dr. Ernest Madsen of the University of Wisconsin and provides tissue-equivalent scanning characteristics of highly scattering, predominantly parenchymal breast tissue. A X-ray CT scan was taken after the manufacture of the breast phantom (Fig. 4c) to benchmark its anatomical structure.

Comparisons of the multi-grid tomography result with that of the standard fixed-grid tomography are shown in Figure 4 for sound speed. Structures in the multi-grid tomograms in Figure 4a and the fixed-grid tomograms in Figure 4b are generally consistent with the X-ray CT image in Figure 4c. The ultrasound scanning position was not exactly matching the position in Fig. 4c, which partially explains the size mismatch of the inclusions between our tomograms and Figure 4c.

Compared to the fixed-grid sound speed image in Figure 4b, the multi-grid sound speed image in Figure 4a contains fewer artifacts. The small inclusions are more visible in Figure 4a, while they are buried in noise in Figure 4b.

### 3.2 In vivo study

To date, over 350 patients have been imaged with our ring array for both sound speed and attenuation distributions within the breast. Here we show two examples (Figure 5 and Figure 6).

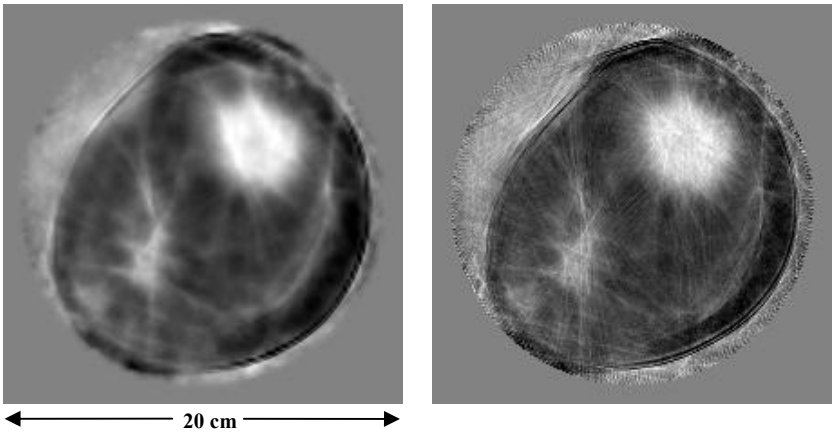


(a) Sound speed reconstruction with the multi-grid tomography

(b) Sound speed reconstruction with the fixed-grid tomography

Figure 5. (a) Sound speed reconstruction with the multi-grid tomography for the breast phantom. (b) Sound speed reconstruction with the fixed-grid tomography for the same cross section as in (a).

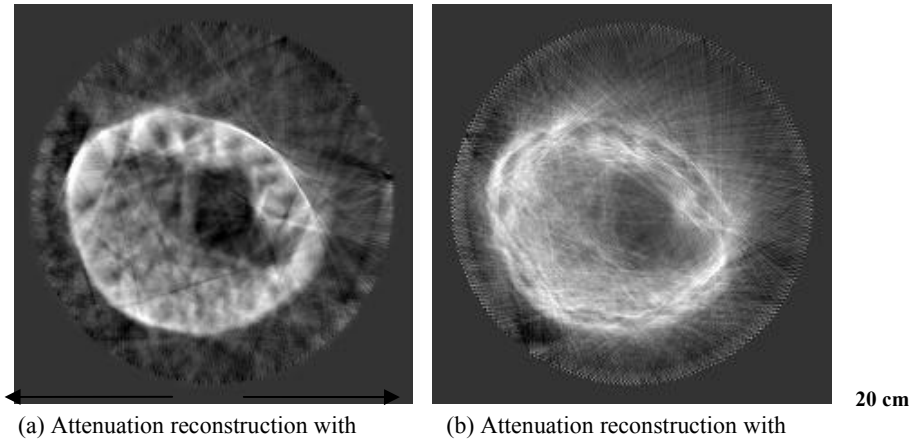


(a) Attenuation reconstruction with the multi-grid tomography

(b) Attenuation reconstruction with the fixed-grid tomography

Figure 6. (a) Attenuation reconstruction with the multi-grid tomography for the breast phantom. (b) Attenuation reconstruction with the fixed-grid tomography for the same cross section as in (a).

One example is presented in Figure 5 for sound speed reconstruction. The breast in Figure 6 shows has a 55 x 47 x 37 mm invasive ductal carcinoma at 12:00 to 1:00 o'clock. The multi-grid sound speed image in Figure 5a shows less contamination from "ray" artifacts when compared the fixed-grid sound speed image in Figure 5b.

In both Figure 5, the edges of the mass at 1:00 to 1:00 o'clock are better delineated in the multi-grid tomograms (Figure 5a) than those in the fixed-grid tomograms (Figure 5b).

Another in vivo example is demonstrated in Figure 6 for attenuation reconstruction. The breast composition is extremely dense. There is a 45 x 46 x 70 mm simple cyst at the 2 o'clock position. The ultrasound characteristics of simple cyst are very close to that of water. Whose ultrasound attenuation is very low when compared to dense breast tissue. Therefore, both attenuation images in Figure 6 clearly show the cyst.

The multi-grid tomogram in Figure 6a exhibit less disturbing artifacts and better reconstructions when compared to the fixed-grid tomograms in Figure 6b. The dense tissue distribution in Figure 6a is much better illustrated than that in Figure 6b. The improvement in image quality by the multi-grid methods is obvious.

## 4. DISCUSSION AND CONCLUSIONS

In this paper we have explained the procedures of using the multi-grid methods to simultaneously reconstruct breast ultrasound sound speed and attenuation images. We have shown some images reconstructed with the multi-grid methods and compared them with the corresponding fixed-grid reconstructions. We need to point out that no regularization has been applied to all the multi-grid tomograms in this paper. However, we did apply regularization to the fixed-grid tomograms to constrain the roughness of the images.

One of the advantages of the multi-grid methods as we mentioned above is that it can effectively reduce the computational cost. For an average patient with total 96 breast ultrasound slices of data, we have compared the number of floating point operations (FLOPs) of the multi-grid method to that of the fixed-grid methods in Table 1. For the comparison in Table 1, we have assumed that, for the multi-grid methods, the forward grid progresses from 128 x 128 to 256 x 256 to 512 x 512, the inverse grid changes from 64 x64 to 128 x 128 to 256 x 256, and there are 5 iterations for the first grid level, 3 iterations for the second grid level and 2 iterations for the final grid level. For the fixed-grid methods, we have taken 512 x 512 as the forward grid and 256 x 256 as the inverse grid for a total of 6 iterations. From Table 1, we can see that the multi-grid methods are able to effectively mitigate the computational burden carried by the fixed-grid methods.

Table 1: Comparison of the number of FLOPs of the multi-grid methods with that of the fixed-grid methods

| Forward grid | Inverse grid | FLOPs for Multi-grid (Trillions) | FLOPs for Fixed-grid (Trillions) |
|---|---|---|---|
| 128 x 128<br>256 x 256<br>512 x512 | 64 x 64<br>128 x 128<br>256 x 256 | 195 (5 iterations)<br>470 (3 iterations)<br>1253 (2 iterations) | n/a<br>n/a<br>3761 (6 iterations) |
| Total FLOPs | | 1918 | 3761 |

Another advantage of the multi-grid tomography methods, as the comparisons show, is that it can effectively limit the presence of artifacts that is associated with over iteration of the fine scale features. As we discussed previously, fine scale features in the breast pose a stricter requirement on the closeness of the starting model to the true model. By starting the inverse process on a coarse grid, we have ignored the fine scale features in the first few iterations and only reconstructed the coarse scale features. This strategy not only speeds up the computation but also provides better starting models for later iterations when the fine scale features gradually kick in, in the inversion process. In other words, the final sound speed and attenuation images reconstructed using the multi-grid methods are insensitive to the initial conditions for the inversion[42].

Another thing we have noted for the multi-grid tomography is that more inversion iterations are needed for the first coarse grid level than later fine grid levels because more efforts are needed to bring the homogeneous starting model closer to the true model.

## ACKNOWLEDGEMENTS

This work was supported in part by a research grant from the Michigan Economic Development Corporation (MEDC653) and Susan G. Komen Breast Cancer Foundation (KG100100).

## REFERENCES

1. M. V. Ranganath, A. P. Dhawan, and N. Mullani, "A multigrid expectation maximization reconstruction algorithm for positron emission tomography," IEEE Trans. Med. Imag., vol. 7, 273–278 (1988).
2. K. Chou, A. Willsky, A. Benveniste, and M. Basseville, "Recursive and iterative estimation algorithms for multi-resolution stochastic processes," in Proc. 28th Conf. Decision and Control, Tampa, FL, Dec. 13-15, 1989, vol. 2, 1184–1189.
3. T. Pan and A. E.Yagle, "Numerical study of multigrid implementations of some iterative image reconstruction algorithms," IEEE Trans. Med. Imag., vol. 10, no. 4, 572–588 (1991).
4. Z. Kato, M. Berthod, and J. Zerubia, "Parallel image classification using multiscale Markov random fields," in Proc. IEEE Int. Conf. Acoustics, Speech, Signal Processing, Minneapolis, MN, Apr. 27–30, 1993, vol. 5, 137–140.
5. Z.Wu, G. T. Herman, and J. A. Browne, "Edge preserving reconstruction using adaptive smoothing in wavelet domain," in Proc. IEEE Nuclear Science Symp. Medical. Imaging Conf., San Francisco, CA, Nov. 6, 1993, vol. 3, 1917–1921.
6. B. Sahiner and A. Yagle, "Image reconstruction from projections under wavelet constraints," IEEE Trans. Signal Process., vol. 41, 3579–3584 (1993).
7. C. A. Bouman and M. Shapiro, "A multiscale random field model for Bayesian image segmentation," IEEE Trans. Image Process., vol. 3, 162–177 (1994).
8. A. Delaney and Y. Bresler, "Multiresolution tomographic reconstruction using wavelets," IEEE Trans. Image Process., vol. 4, no. 6, 799–813 (1995).
9. G.Wang, J. Zhang, and G. Pan, "Solution of inverse problems in image processing by wavelet expansion," IEEE Trans. Image Process., vol. 4, 579–591 (1995).
10. H.-C. Yang and R. Wilson, "Adaptive image restoration using a multiresolution Hopfield neural network," in Proc. 5th Int. Conf. Image Processing and its Applications, Edinburgh, U.K., Jul. 4–6, 1995, 198–202.
11. M. Bhatia, W. C. Karl, and A. S. Willsky, "Wavelet-based method for multiscale tomographic reconstruction," IEEE Trans. Med. Imag., vol. 15, 92–101 (1996).
12. S. S. Saquib, C. A. Bouman, and K. Sauer, "A non-homogeneous MRF model for multiresolution Bayesian estimation," in Proc. IEEE Int. Conf. Image Processing, Lausanne, Switzerland, Sep. 16–19, 1996, vol. 2, 445–448.
13. W. Zhu, Y. Wang, Y. Deng, Y. Yao, and R. Barbour, "A waveletbased multiresolution regularization least squares reconstruction approach for optical tomography," IEEE Trans. Med. Imag., vol. 16, 210–217 (1997).
14. E. L. Miller, L. Nicolaides, and A. Mandelis, "Nonlinear inverse scattering methods for thermal wave slice tomography: A wavelet domain approach," J. Opt. Soc. Amer. A, vol. 15, 1545–1556 (1998).
15. R. Nowak and E. D. Kolaczyk, "A multiscale MAP estimation method for Poisson inverse problems," in Proc. 32nd Asilomar Conf. Signals, Systems, Computers, Pacific Grove, CA, Nov. 1-4, 1998, vol. 2, 1682–1686.
16. R. D. Nowak, "Shift invariant wavelet-based statistical models and 1/f processes," presented at the IEEE DSP Workshop (1998).
17. M. L. Comer and E. J. Delp, "Segmentation of textured images using a multiresolution Gaussian autoregressive model," IEEE Trans. Image Process., vol. 8, 408–420 (1999).

18. J.-M. Laferte, P. Perez, and F. Heitz, "Discrete Markov image modeling and inference on the quadtree," IEEE Trans. Image Process., vol. 9, 390–404 (2000).

19. R. D. Nowak and E. D. Kolaczyk, "A statistical multiscale framework for Poisson inverse problems," IEEE Trans. Inf. Theory, vol. 46, 1811–1825 (2000).

20. N. Lee and B. J. lucier, "Wavelet methods for inverting the radon transform with noisy data," IEEE Trans. Image Process., vol. 10, 79–94 (2001).

21. T. Frese, C. A. Bouman, and K. Sauer, "Adaptive wavelet graph model for Bayesian tomographic reconstruction," IEEE Trans. Image Process., vol. 11, 756–770 (2002).

22. A. B. Milstein, S. Oh, J. S. Reynolds, K. J.Webb, C. A. Bouman, and R. P. Millane, "Three-dimensional Bayesian optical diffusion tomography using experimental data," Opt. Lett., vol. 27, 95–97 (2002).

23. S. Oh, A. B. Milstein, R. P. Millane, C. A. Bouman, and K. J. Webb, "Source-detector calibration in three-dimensional Bayesian optical diffusion tomography," J. Opt. Soc. Amer. A, vol. 19, 1983–1993, (2002).

24. A. B. Milstein, S. Oh, K. J. Webb, C. A. Bouman, Q. Zhang, D. A. Boas, and R. P. Millane, "Fluorescence optical diffusion tomography," Appl. Opt., vol. 42, 3081–3094, (2003).

25. O. H. Seungseok, C. A. Bouman and K. J. Webb, "Multigrid Tomographic Inversion with Variable Resolution Data and Image Spaces," IEEE Trans. Imag. Proc., Vol 15, 2805-2819 (2006).

26. A. Brandt, "Multi-level adaptive solutions to boundary value problems,"Math. Comput., vol. 31, 333–390 (1977).

27. W. L. Briggs, V. E. Henson, and S. F. McCormick, A Multigrid Tutorial, 2nd ed. Philadelphia, PA: SIAM, 2000.

28. C. A. Bouman and K. Sauer, "Nonlinear multigrid methods of optimization in Bayesian tomographic image reconstruction," in Proc. SPIE Conf. Neural and Stochastic Methods in Image and Signal Processing, San Diego, CA, Jul. 19–24, 1992, vol. 1766, 296–306.

29. S. F. McCormick and J. G. Wade, "Multigrid solution of a linearized, regularized least-squares problem in electrical impedance tomography," Inv. Probl., vol. 9, 697–713 (1993).

30. V. E. Henson, M. A. Limber, S. F. McCormick, and B. T. Robinson, "Multilevel image reconstruction with natural pixels," SIAM J. Sci. Comput., vol. 17, 193–216 (1996).

31. C. R. Johnson, M. Mohr, U. Ruede, A. Samsonov, and K. Zyp, , T. J. Barth, T. F. Chan, and R. Haimes, Eds., "Multilevel methods for inverse bioelelectric field problems," in Lecture Notes in Computational Science and Engineering – Multiscale and Multiresolution Methods: Theory and Applications. Heidelberg, Germany: Springer-Verlag, 2001, vol. 20.

32. J. C. Ye, C. A. Bouman, R. P. Millane, and K. J. Webb, "Nonlinear multigrid optimization for Bayesian diffusion tomography," presented at the IEEE Int. Conf. Image ProcessingKobe, Japan, Oct. 25–28, 1999. [33] J. C. Ye, C. A. Bouman, K. J. Webb, and R. P. Millane, "Nonlinear multigrid algorithms for Bayesian optical diffusion tomography," IEEE Trans. Image Process., vol. 10, 909–922 (2001).

33. A. Brandt, "Multiscale and multiresolution methods: Theory and applications," in Multiscale Scientific Computation: Review 2001, T. J. Barth, T. F. Chan, and R. Haimes, Eds. Heidelberg, Germany: Springer-Verlag, 2001, 3–96.

34. A. Brandt and R. Gandlin, "Multigrid for atmospheric data assimilation: Analysis," in Proc. Hyperbolic Problems: Theory, Numerics and Applications, Pasadena, CA, Mar. 2002, 369–376.

35. A. Brandt and D. Ron, "Multigrid solvers and multilevel optimization strategies," in Multilevel Optimization and VLSICAD, J. Cong and J. R. Shinnerl, Eds. Boston, MA: Kluwer, 2002, 1–69.

36. R. Gandlin and A. Brandt, "Two multigrid algorithms for inverse problem in electrical impedance tomography," presented at the Copper Mountain Conf. Multigrid Methods Copper Mountain, CO, Mar. 30-Apr. 4, 2003.

37. J. A. O'Sullivan and J. Benac, "Alternating minimization multigrid algorithms for transmission tomography," in Proc. SPIE Conf. Computational Imaging II, San Jose, California, Jan. 2004, 216–21.

38. S. Oh, A. B. Milstein, C. A. Bouman, and K. J.Webb, "Ageneral framework for nonlinear multigrid inversion," IEEE Trans. Image Process., vol. 14, 125–140 (2005).

39. C. Li, N. Duric, N., "In vivo breast sound-speed imaging with ultrasound tomography," Ultrasound in Med. & Biol., 35, 1615-1628 (2009).

40. J. Nocedal, S. J. Wright, "Limited-Memory Quasi-Newton Methods: Numerical Optimization," Springer, 2nd ed. New York: Mikosch TV, Resnich SI, Robinson SM (2000).

41. C. C. Paige and M. A. Asunders, "LSQR: An Algorithm for Sparse Linear Equations and Sparse Least Squares,", ACM Trans. On Math. Softw., Vol. 8, 43-71 (1982).

42. J. K. Washbourne, K. P. Bube, P. Carillo and C. Addington, "Wave tracing: Ray tracing for the propagation of band-limited signals: Part2 – Applications," Geophysics, Vol. 73, 385-393 (2008).